Engineering with Computers
https://doi.org/10.1007/s00366-023-01917-5

ORIGINAL ARTICLE

Response of an Euler–Bernoulli beam subject to a stochastic disturbance

Lukman Olawale[1] · Tao Gao[2] · Erwin George[1] · Choi-Hong Lai[1]

Received: 2 October 2022 / Accepted: 26 October 2023

Abstract
This work concerns the stochastic analysis of the bending of a slender cantilever beam subject to an external force with the inclusion of a stochastic effect characterised by white noise. The beam deflection is governed by the classic dynamic Euler–Bernoulli equation. Its response to the stochastic external load is investigated by learning pattern from the simulation data which are collected from numerical computations of ten thousand numerical experiments, which are achieved using a finite difference method coupled with a Monte Carlo method for the uncertainty quantification. Insightful results are presented with visualisation techniques and discussed in detail. Of note, by performing regression analysis to the data, the solution is shown to follow a centred Gaussian process with a strong numerical evidence. The associated autocovariance matrix is computed using the sample data. Then, a mild solution in the probability sense for the deflection at a fixed position and a fixed time is written explicitly in a simple form. The results obtained by the finite difference scheme were also compared to the finite-element scheme and were found to be in good agreement. Unsurprisingly, the finite-element scheme was found to be much more computationally expensive compared to finite difference scheme. Hence, for such a simple structure, the stochastic analysis using the finite difference scheme is preferred. Analysis of the results also showed that some of the regression parameters converge when the number of simulations reaches five hundred and only vary subject to numerical errors of order 10^{-6} if the number of simulations is further increased. While others converge when the number of simulations exceeds two thousand showing that depending on the level of precision required fewer than ten thousand simulations might be required.

Keywords Euler–Bernoulli beam · Stochastic partial differential equation · Finite difference · Monte Carlo simulation · Stochastic process · Regression · Machine learning · Visualisation

1 Introduction

It has been more than two centuries since the introduction of the Euler–Bernoulli beam theory by two famous mathematicians in 1750, which is a linear partial differential equation (PDE) in one-dimensional space and time characterising small deflections of an uniform beam subject to a lateral load. The simplest form is

$$EI\frac{\partial^4 w}{\partial y^4} + \mu\frac{\partial^2 w}{\partial t^2} = Q(y,t), \tag{1}$$

where w is the deflection in the lateral direction, y is the longitudinal spatial variable, t is the time variable, Q is the load distribution, μ is the mass per unit length, E is the Young's modulus, and I is the second moment of the area of the beam's cross section. The product EI is known as the flexural rigidity denoted by D that measures the force required to bend the beam. The Euler–Bernoulli beam theory was widely applied at different scales in many areas. It was used to study the weight-bearing bones of human body in biomechanics, as well as the design and analysis of a wide range of structures, such as cable-stayed bridges, roofs of football stadia, high-rise buildings, etc. The research interest arose from the potential risk of the structures being damaged by external strong forcing (e.g., earthquake or wind load in architectural engineering). Therefore, an in-depth

✉ Lukman Olawale
l.o.olawale@greenwich.ac.uk

✉ Tao Gao
t.gao@essex.ac.uk

[1] School of Computing and Mathematical Sciences, University of Greenwich, London SE10 9LS, UK

[2] School of Mathematics, Statistics and Actuarial Science, University of Essex, Colchester CO4 3SQ, UK

Published online: 24 November 2023

understanding of such vibration through the use of novel mathematical tools has always been essential in the relevant engineering designs. In particular, an important topic is modelling the effect of wind loads on high-rise buildings in which much work has been done so far (see, e.g., [14–16] and the references therein).

Randomness is inevitable in the nature. For example, the pressure load acting on the large-scale structure presents stochastic features due to the fluid flow around complex structures and possible minor inhomogenity of materials at different manufacturing stages. Also, physical quantities, such as surface density and material properties of a building, may change gradually due to long-term weathering and erosion caused by wind and rain. Hence, it is reasonable, and of significant interest to include stochastic effect in the mathematical modelling of certain physical processes to address the randomness in these phenomena. One usually ends up with a partial differential equation in the presence of stochastic coefficients and source terms called stochastic partial differential equation [10]. Over the years, the most studied cases are the stochastic heat equation (see, e.g., [2, 6]), which is a linear partial differential equation with a simple explicit Green's function usually referred to as the heat kernel, and the stochastic Burger's equation (see, e.g., [3]) which is the simplest nonlinear partial differential equation. Existing work and literature in the stochastic Euler–Bernoulli equation are limited to the author's knowledge. This work focuses on the investigation of a stochastic Euler–Bernoulli Equation (1) when

$$Q(y,t) \propto \xi(y,t), \tag{2}$$

in which $\xi(y,t)$ is a Gaussian white noise which can be used for the stochastic analysis of the deflection behaviour of slender structures, such as high-rises, sky scrapers, and a new kind of wind turbine, namely, the Bladeless Wind Turbine (BWT) subjected to Gaussian excitation.

To reduce the complexity of the study, a beam built into a fixed foundation base on the ground level itself may be regarded as a simplified realisation of a large-scale architecture. Assuming that there is no erosion at the ground level, the deflection of a cantilever in the framework of the Euler–Bernoulli beam theory subject to stochastic external loading is examined. Such a method of reducing the order of the problem had been done, for example in [7, 8] for static analysis using the Timoshenko beam theory, where a high-rise building is modelled in a simplified form as a cantilever structure. Even more pertinent is the modelling of a Bladeless Wind Turbine (BWT) as a cantilever structure, because the reduced model is much closer to the real world. BWT is a particularly important and interesting new class of turbine due to its simple structure which confers advantages, such as ease of manufacturing, transportation, storage, and installation. It is also easier to maintain, because it lacks bearings, gears, and other moving parts. The new turbine also lacks the the environmental hazards associated with conventional wind turbines, such as collision of birds with blades of the turbines. It can be used offshore, in a wind farm or wherever high-intensity winds exist.

Several studies have examined the structural response of BWT turbines using the Euler–Bernoulli beam theory. For instance, Bahadur [1] studied the dynamics of a tunable BWT. There is an interest in tuning the frequency of vibration of a BWT to match the vortex shedding frequency that is created due to flow around the body of the BWT. Such tuning results in the resonant vibration of the BWT, the so-called lock-in effect [17], thereby increasing the power output. Another study [4] looked at the Fluid–Structure Interaction (FSI) with the aim of developing tools needed to simulate FSI problem as it relates to BWTs so as to reproduce experimental results for scaled models of BWTs using the Alya system, a multi-physics code developed in the Barcelona Supercomputing Center [20]. Chizfahm [5] studied the dynamic response as well as the FSI of a BWT by examining the different shapes and configurations of the BWT structure. Using the Euler–Bernoulli beam theory combined with aero-dynamic models of the forces of the structures, Chizfahm proposed a model for each of the configurations of the BWT. The models were validated through comparison with a 3D CFD-FEM numerical simulation. The effects of the wind speed on the induced lift force, deflection, and generated power of the different shapes of the BWTs were investigated.

The aforementioned studies have focused on the structural analysis and the FSI studies of a BWT in a deterministic manner. Given the important benefit of this new class of wind turbine, and the fact that wind flow is in fact stochastic in nature, this study sets out to analyse the deflection characteristics of these kinds of structures using the theory of stochastic processes in the framework of the Euler–Bernoulli equation.

The present study is restricted to two-dimensional physical space with particular attention to the response to the forcing load applied in the lateral direction in the presence of a stochastic effect. In spite of the simplification, solving the stochastic Euler–Bernoulli equation is still very challenging. To discover the solution behaviour in simple form, computational data are simulated in 10,000 numerical experiments achieved by a finite difference (FD) scheme, and used for pattern learning by means of regression.

The paper is structured as follows. The mathematical formulation is sketched in Sect. 2 followed by the Finite Difference numerical scheme in Sect. 3. The computational data and the machine learning are presented in Sect. 4. The numerical results achieved by the Finite Difference Method (FDM) are compared to the ones achieved by a

Finite-Element Method (FEM) in Sect. 5. A conclusion is made in Sect. 6.

2 Formulation

A beam of length h with uniform density and flexural rigidity is considered under the effect of a pressure load. Its lower end is assumed to be anchored as a fixed end at the ground floor, while the top is free to move. The bending of the beam is governed by the so-called Euler Bernoulli equation.

The problem is formulated in a two-dimensional Cartesian coordinate system. The pressure load follows the positive x-direction. The origin O is set at the fixed end of the beam. The displacement of the beam is denoted by $x = w(y, t)$. An illustrating schematic is presented in Fig. 1.

For the sake of easy notations, a prime $'$ is used to denote the partial derivative of the displacement with respect to y, and $\cdot$ is used to denote the partial derivative of the displacement with respect to t. By choosing

$$h, \quad \sqrt{\frac{\mu h^4}{D}}, \quad \frac{D}{h^4}, \tag{3}$$

as the reference length, time, and pressure, respectively, the governing equation for the bending of the beam is

$$w'''' + \ddot{w} = q(y, t), \tag{4}$$

where $q(y, t)$ is the scaled external load. The boundary conditions for a cantilever beam are

$$w(0, t) = w'(0, t) = w''(1, t) = w'''(1, t) = 0. \tag{5}$$

The conditions at $y = 1$ are based on the assumption of no bending moment and no shearing force at the free end of the beam respectively. For an initial value problem (IVP), the beam is assumed to be initially at rest, so

$$w(y, 0) = \dot{w}(y, 0) = 0. \tag{6}$$

In the presence of a stochastic disturbance characterised by a white noise in the external load, one may rewrite the load q as

$$q(y, t) = q_0(y, t) + \tilde{\sigma}\xi(y, t), \tag{7}$$

in which q_0 is the deterministic load and ξ is a standard Gaussian white noise with respect to time and space, where

$$\mathbb{E}\left[\xi(y_1, t_1)\xi(y_2, t_2)\right] = \delta_{y_1,y_2}\delta_{t_1,t_2}. \tag{8}$$

Here, δ is the Kronecker delta function defined by

$$\delta_{m,n} = 1, \qquad \text{if } m = n, \tag{9}$$

$$\delta_{m,n} = 0, \qquad \text{otherwise.} \tag{10}$$

And $\tilde{\sigma}$ is a parameter that measures the standard deviation of the white noise. Due to the linearity, the response to the stochastic effect, denoted by $\tilde{w}$, also satisfies the governing equation

$$\tilde{w}'''' + \ddot{\tilde{w}} = \tilde{\sigma}\xi(y, t). \tag{11}$$

The value of $\tilde{\sigma}$ can be selected to be 1 without losing generality, and the tildes are dropped to ease the notations. It yields the stochastic Euler–Bernoulli equation

$$w'''' + \ddot{w} = \xi(y, t). \tag{12}$$

The rest of the work is to explore the form of the solution to (12). A linear theory of modal decomposition can be developed to solve the special case where the white noise is spatial invariant, i.e., it depends on time only. The detail is presented in Appendix 1 for readers who are interested. Full computations are required to investigate the general case. They will be achieved by a numerical scheme based on a Finite Difference Method (FDM) coupled with backward time integration, which is to be introduced in the next section.

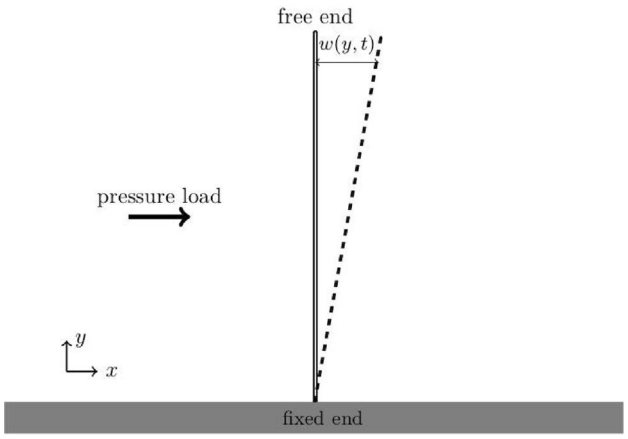

Fig. 1 Schematic of the two-dimensional problem. The solid line depicts the undisturbed slender beam. The dashed curve shows the deflection

3 Numerical scheme

To investigate the stochastic feature in which thousands of numerical experiments are to be conducted, a fast efficient numerical scheme is required. To this end, FDM is preferable over commonly used Finite-Element Method (FEM) for its less computational cost. A valid scheme to solve the time-dependent Euler–Bernoulli equation is presented in this

section. The physical domain is uniformly discretised into N grid points

$$y_i = \frac{i}{N}, \quad i = 1, 2, ..., N, \tag{13}$$

and

$$w_i = w(y_i), \quad i = 1, 2, ..., N. \tag{14}$$

In particular, $y = 0$ and $y = 1$ represent the fixed end and the free end atop, respectively. The discretised unknown vector is denoted by $\mathbf{W}$, i.e., $\mathbf{W} = [w_1, w_2, ..., w_N]^T$. To accommodate the boundary conditions (5), four ghost points are introduced

$$y_{-1} = -\frac{1}{N}, \quad y_0 = 0, \quad y_{N+1} = 1 + \frac{1}{N}, \quad y_{N+2} = 1 + \frac{2}{N}. \tag{15}$$

By imposing second-order accurate FD scheme for the boundary conditions in (5), one obtains

$$w_0 = 0, \tag{16}$$

$$w_{-1} = w_1, \tag{17}$$

$$w_{N+1} = 2w_N - w_{N-1}, \tag{18}$$

$$w_{N+2} = w_{N-2} - 4w_{N-1} + 4w_N. \tag{19}$$

A matrix of the central FD scheme for w over $\{y_i\}_{i=1,2,...,N}$ subject to (16)–(19) can be written.

The dynamics of (4) is computed numerically using a backward difference in time, e.g., the Implicit Euler method, and a central difference of second order in space. By introducing an artificial variable $v = \dot{w}$, Eq. (4), which is second order in time, can be rewritten as two coupled PDEs of first order

$$\frac{\partial U}{\partial t} = MU + F, \tag{20}$$

where

$$U = \begin{pmatrix} w \\ v \end{pmatrix}, \qquad M = \begin{pmatrix} 0 & 1 \\ -\frac{\partial^4}{\partial y^4} & 0 \end{pmatrix}, \quad F = \begin{pmatrix} 0 \\ q \end{pmatrix}. \tag{21}$$

The time domain $[0, T]$, where T is the final time, is divided into n steps with $\Delta t = T/n$. By discretising spatially in y and temporally in t, the discretised variables are denoted as

$$\mathbf{U}_i^j = \begin{pmatrix} w(y_i) \\ v(y_i) \end{pmatrix}, \quad \text{at } t = t_j = \frac{jT}{n}. \tag{22}$$

The backward Euler scheme can then be written in the matrix form

$$\begin{pmatrix} I_N & -\Delta t I_N \\ \Delta t \mathcal{M} & I_N \end{pmatrix} \begin{pmatrix} \mathbf{W^{j+1}} \\ \mathbf{V^{j+1}} \end{pmatrix} = \begin{pmatrix} \mathbf{W^j} \\ \mathbf{V^j} \end{pmatrix} + \begin{pmatrix} 0 \\ \mathbf{Q}\Delta t \end{pmatrix}, \tag{23}$$

where I_N is the identity matrix and $\mathcal{M}$ is the matrix containing FD replacement of the fourth derivative with respect to s. Vector $\mathbf{V} = [v_1, v_2, ..., v_N]^T$ and $\mathbf{Q} = [q_1, q_2, ..., q_N]^T$ are defined in a similar manner to (14). Multiplying both sides by the inverse of the matrix from the left-hand side completes one time increment of the backward scheme. The numerical stability is guaranteed due to the nature of the implicit method. For higher accuracy, $\Delta y = 0.005$ and $\Delta t = 0.04$ are chosen in all the simulations.

– To validate the numerical scheme, we consider an example of deterministic pressure as follows. A time-varying load under the form of

$$p(y, t) = \sin(\omega_f t), \tag{24}$$

can be considered as the excitation due to vortex shedding [11, 19], where the frequency ω_f depends on the cross-sectional geometry, the flow velocity, and the Strouhal number. The vortex-induced vibration in the frequency domain is

$$\hat{w} = i\pi \int_0^1 g(y, \eta, \omega)\Big(\delta(\omega - \omega_f) - \delta(\omega + \omega_f)\Big)d\eta, \tag{25}$$

in which g is the Green's function for the Euler–Bernoulli equation in the frequency domain first pioneered by [9] and summarised by [18]. Calculating the inverse Fourier transform of (25) yields

$$w = \sin(w_f t) \int_0^1 g(y, \eta, w_f)d\eta. \tag{26}$$

Hence, the dynamic response of the beam to the periodic load oscillates with the same frequency. The parameters for the numerical experiments are chosen as $\omega_f = \pi/5$. Solution (26) is evaluated up to $t = 100$ and compared with the computation by the FD scheme. The results are found to match well. The single-sided Fourier spectrum of the dynamics at the beam tip ($y = 1$) is shown in Fig. 2 where the dominant frequency is found to be exactly the same as that of the load.

The numerical test presented above demonstrated good agreement between the analytical and numerical results, which validates the code based on the numerical scheme for the above Euler–Bernoulli problem. We follow to employ the numerical scheme to compute the dynamics of (12).

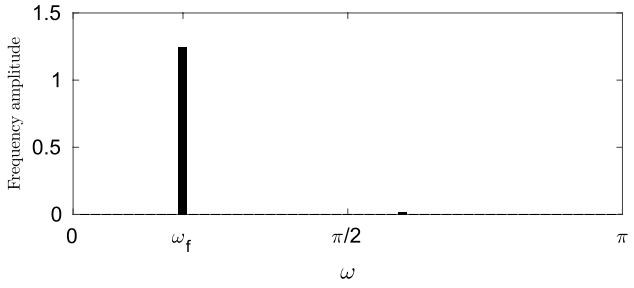

Fig. 2 Fourier spectrum of the response to the load (24) on the top of the beam with $\omega_f = \pi/5$ and $F(y) = 1$ computed by the FD scheme

4 Computational results and analysis

The computations are achieved by employing the numerical scheme introduced in Sect. 3 and letting $Q = [\psi_1, ..., \psi_N]^T$ in (23), where

$$\psi_j = \frac{X}{\sqrt{\Delta t}}, \quad j = 1, 2, ..., N, \tag{27}$$

is the discretised stochastic load. Here, X is a random variable following the standard normal distribution, i.e., $X \sim N(0, 1)$. The uncertainties in the solution of the stochastic Euler–Bernoulli Equation are quantified using the simulation data obtained from the Monte Carlo method whereby 10,000 numerical experiments are conducted. It is found that the statistics of the deflections remains the same from time $t > 20$ onward. Hence, it is appropriate to select $T = 20$ as the final time in the computations hereafter.

The numerical outputs at the end of the experiments are presented in Fig. 3 showing all the beam deflections from the 10,000 simulations, the mean and the variance, and the standard error of the Monte Carlo Method. As can be seen from that figure, the profiles in the top left panel are smooth and symmetric by the undisturbed state. The mean displacement is very close to zero as predicted by the linear theory (61) from the appendix.

To get more intuition on the solution by making full use of the data, machine learning by means of regression is to be conducted and proceeded in four steps as follows.

1. At a fixed position and a fixed time, the behaviour of the beam displacement w can be described by a probability

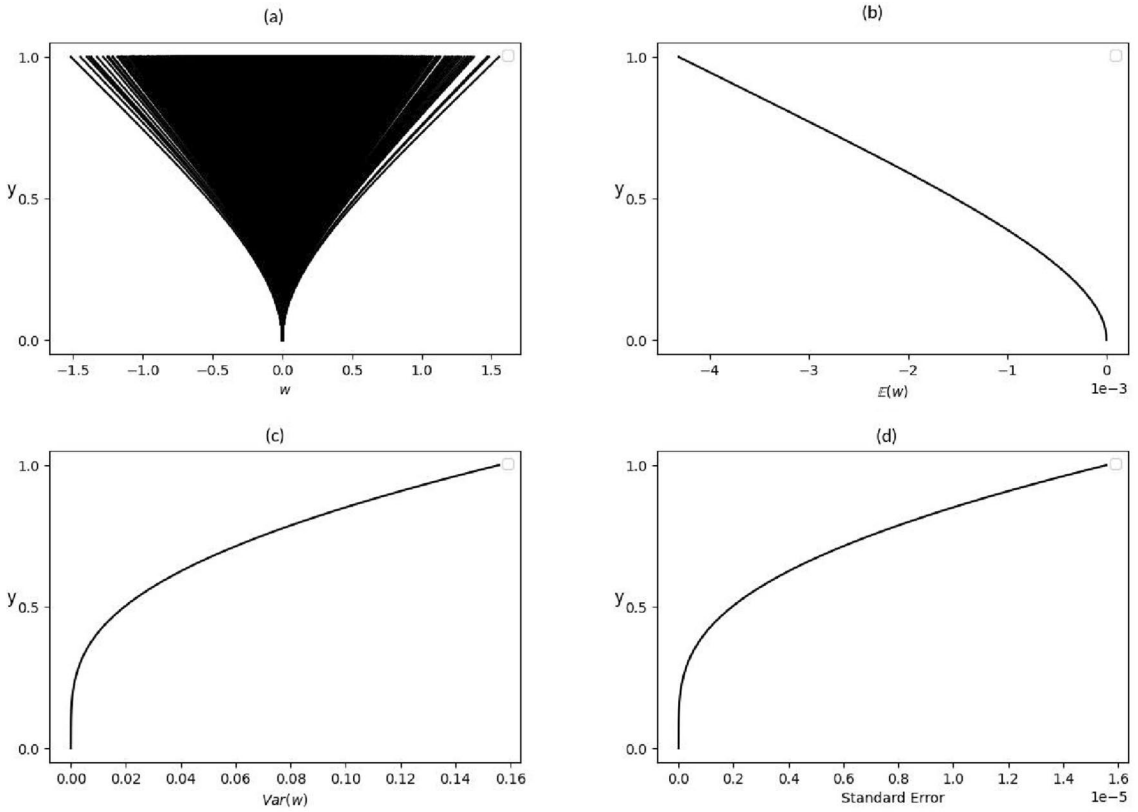

Fig. 3 **a** Snapshots of w due to stochastic load in (12) using Monte Carlo method at $t = 20$. **b** Expectation $\mathbb{E}$ of the stochastic process at $t = 20$ along the beam. **c** Variance of the stochastic process at $t = 20$ along the beam. **d** Standard error of the Monte Carlo method at $t = 20$ along the beam

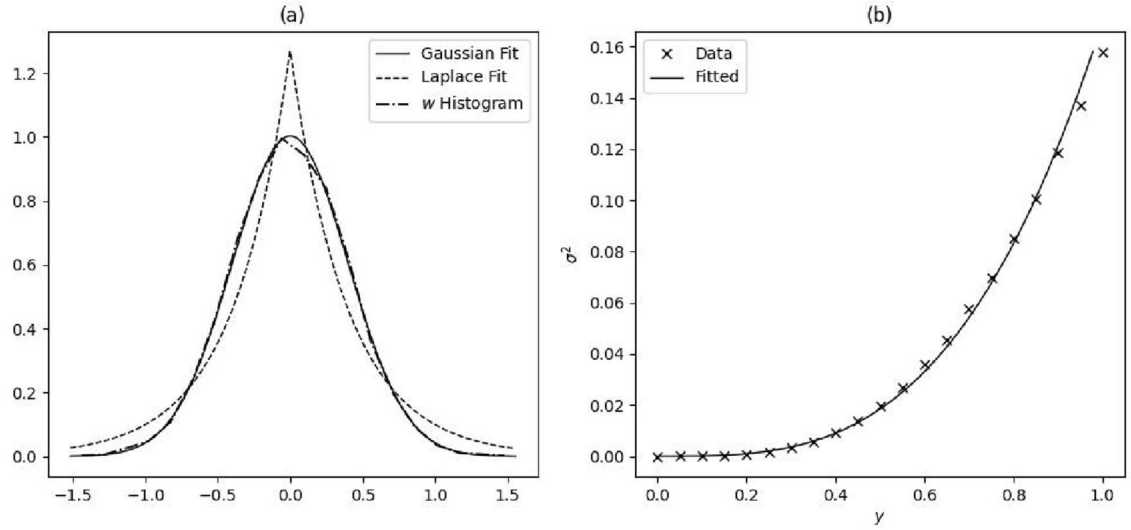

Fig. 4 **a** Various distribution fitted to the deflection data recorded at the beam tip at $t = T$. **b** The variance for various points on the beam at $t = T$ and the fitted curve

distribution. The simulation data of 10,000 experiments are then fitted to different candidates, and two best fittings of the deflection data at the tip of the beam at the final time are depicted in Fig. 4a, indicating that the data have a great match with a Gaussian distribution. This process has been repeated at different positions or different times, and qualitatively similar results are obtained. It is a strong numerical evidence showing that w follows a normal distribution at a given time and position. The two Gaussian parameters $\mu(y,t)$ (the mean) and $\sigma^2(y,t)$ (the variance) can be both estimated by the sample data. The former is close to zero at all y and all t as previously discussed. The latter is shown in Fig. 4 when $t = T$ and for various positions on the beam.

2. As w is Gaussian at a given time and position, it can be shown that, in general, w is a multi-dimensional (centred) Gaussian process. The remaining task is to study the associated covariance/correlation matrix. An algebraic growth of the variance in y is observed from Fig. 4b. It suggests a model for the standard deviation of the following form:

$$\sigma(y,t) = \lambda y^{\alpha}, \quad \text{at } t = T, \tag{28}$$

in which λ and α are the parameters to estimate by using the least-squares method. The result is shown in Fig. 4b, and the values of the estimated parameters are listed in Table 1. For better understanding the statistics of the solution, the spatial covariance and correlation matrices, denoted by K_{yy} and ρ_{yy}, respectively, for various points along the beam at a fixed time are computed using the simulation data. For a direct visualisation of the spatial covariance matrix, a colour-map image representation is introduced as in Fig. 5. The darker pixels close to the top right corner of the image correspond to higher covariance of points close to the free end of the beam, whereas the brighter pixels on the bottom left are for those in the vicinity of the fixed end with lower covariance. The result is very convincing as the covariance near the bottom is restricted to be almost zero due to the boundary condition imposed for an anchored

Table 1 The values of estimated parameters for the data at $t = T$

Parametric estimations	
$\tilde{\lambda}$	$\tilde{\alpha}$
1.7405	0.6250

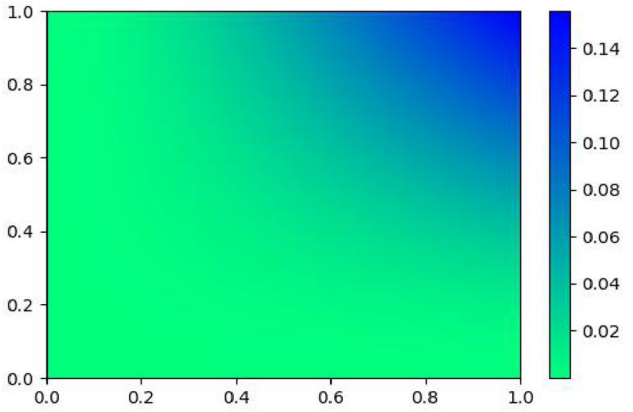

Fig. 5 Colour-map image representation of the covariance matrix at time $t = T$ (colour online)

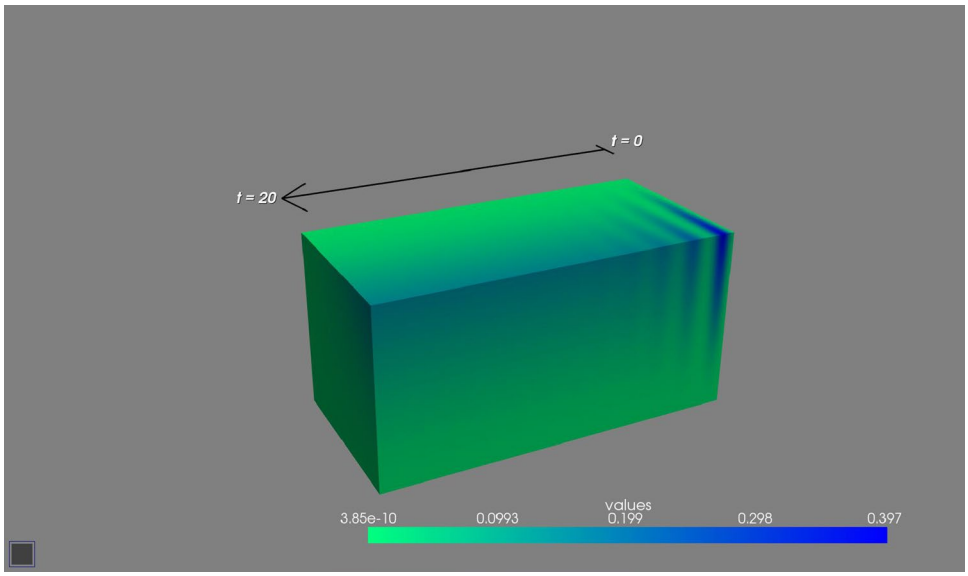

Fig. 6 3D colour-map representation of the covariance matrix at discrete time $t = 0$ to $t = T$ (colour online)

Table 2 The values of estimated parameters for model (29) at the top end

Parametric estimations		
$\tilde{\beta}$	$\tilde{\gamma}$	$\tilde{\Omega}$
−0.6461	0.9169	3.4855

base. This calculation has been repeated for other times, and the obtained pictures are stacked up along the time variable t to form a three-dimensional colour-map image as in Fig. 6. It is observed that the spatial covariance decays with oscillation in time and tends to a fixed value in long term. On the other hand, the correlation matrix is found to be of a unit matrix (matrix of ones), illustrating that the beam deflection is (perfectly) positively spatially correlated at the final time. Qualitatively similar results have been discovered at other time.

3. Some interesting features have been observed in Fig. 6. For a full comprehension of the decaying oscillatory behaviour of the spatial covariance, the second step of the pattern learning is to investigate the temporal covariance by conducting regression analysis to the data at a given position, e.g., the top end of the beam, for different times. The sample temporal variance is plotted in Fig. 7 in which the nature of exponential decay with oscillations is confirmed. Then, a model for the standard deviation is proposed as follows:

$$\sigma(y,t) = \sigma^*(y)\left(1 - e^{\beta t^\gamma}\cos \Omega t\right), \qquad \text{at } y = 1, \tag{29}$$

where $\sigma^*(y)$ is the limit of $\sigma(y,t)$ for large t, and β, γ, and Ω are the parameters to estimate by the least-squares approach. The estimations are shown in Table 2. The regression analysis has been also conducted at other positions such as $y = 1/4$, $y = 1/2$, and $y = 3/4$. It is

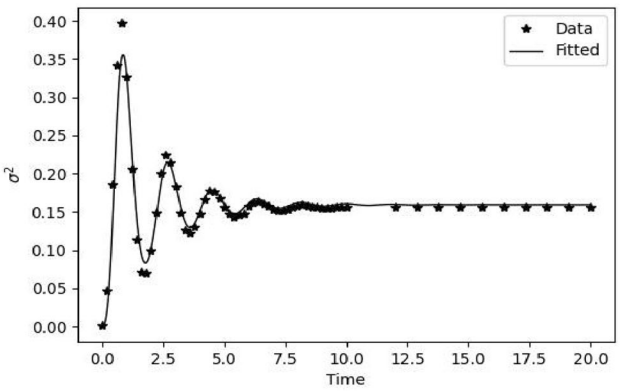

Fig. 7 Standard deviation at the top of the beam from time $t = 0$ to $t = T$

discovered that there is hardly any change in the estimation of the three parameters at various positions, which indicates that β, γ, and Ω are in fact spatial invariant. Then, it can be readily shown that $\sigma^*(y)$ takes the form of (28), that is

$$\sigma^*(y) = \lambda y^\alpha. \tag{30}$$

Next, in a manner similar to the previous step, we compute the temporal covariance and correlation matrix, denoted by K_{tt} and ρ_{tt}, respectively, from the sample data at the top end for various times. The former is displayed as a colour-map image in Fig. 8. It can be clearly seen that the temporal covariance converges to a limit with oscillations in long term. This calculation has been repeated for different positions along the beam. Using the same visualisation technique of stacking up the colour-map images, a three-dimensional colour-map

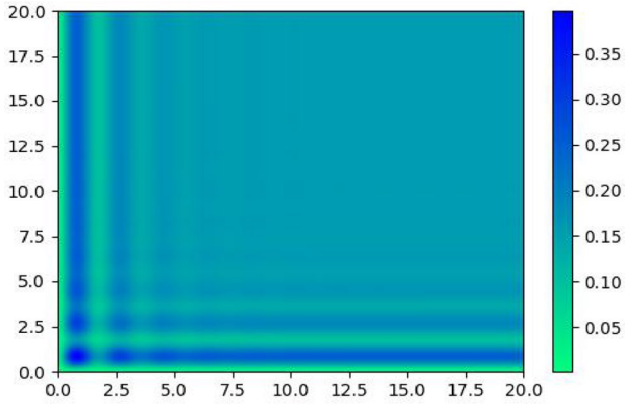

Fig. 8 Colour-map image representation of the temporal covariance matrix at $y = 1$ (colour online)

representation is formed and plotted in Fig. 9 that provides a clear view on the overall evolution of the temporal covariance. On the other hand, the temporal correlation matrix is again found to be of a unit matrix, showing that the beam deflection is (perfectly) positively temporally correlated at a fixed position.

4. Combining the results obtained from the previous three steps, it can be concluded that $w(y, t)$ follows a centred Gaussian process whose covariance function is written as:

$$C(y_1, y_2, t_1, t_2) = \lambda^2 y_1^{\alpha} y_2^{\alpha} (1 - e^{\beta t_1^{\gamma}} \cos \Omega t_1)(1 - e^{\beta t_2^{\gamma}} \cos \Omega t_2), \quad (31)$$

in which the estimations of the parameters from the simulation data are listed in Tables 1 and 2. In particular, at a given time and a given position, the standard deviation of the deflection is written as

$$\sigma(y, t) = \lambda y^{\alpha} (1 - e^{\beta t^{\gamma}} \cos \Omega t), \quad (32)$$

or simply $w(y, t) \sim N(0, \sigma(y, t)^2)$, that is a simple-form mild solution to the stochastic Euler–Bernoulli equation in the probability sense.

Figures 10 and 11 show the convergence history of the parameters. All the parameters are found to converge when the number of simulations is sufficiently large. In particular, α, β, γ, and ω converge when this number reaches 500 and only vary subject to numerical errors of order 10^{-6} if the number of simulations is further increased. Meanwhile, the convergences of λ and σ^* are achieved when the number of simulations exceeds 2000.

5 Result verification

In this section, we compare the results obtained by the FDM to FEM. To achieve this, we seek an approximate solution to the Euler–Bernoulli equation of the form

$$w(y, t) = \sum_{j}^{N} w_j(t) \eta_j(y), \quad (33)$$

where the $\eta_j(y)$ terms are some bases or interpolation functions at the nodes j. Suppose the Euler–Bernoulli PDE operator is written as $\mathcal{L}(w) = \frac{\partial^4 w}{\partial y^4} + \frac{\partial^2 w}{\partial t^2} - q = 0$, and then, the residual of the approximate solution is

$$R = \mathcal{L}\left(\sum_{j}^{N} w_j \eta_j \right). \quad (34)$$

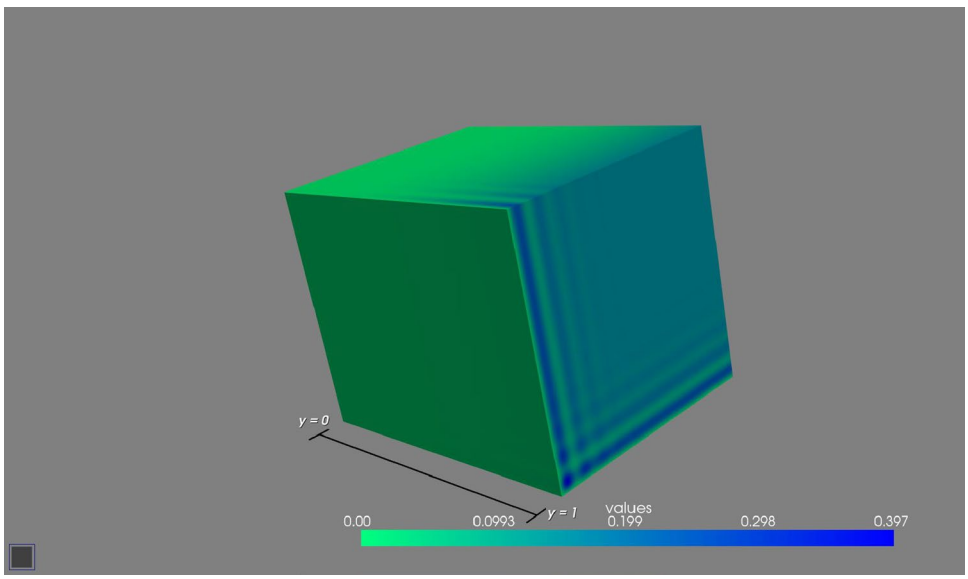

Fig. 9 3D colour-map representation of the temporal covariance matrix from $y = 0$ to $y = 1$ (colour online)

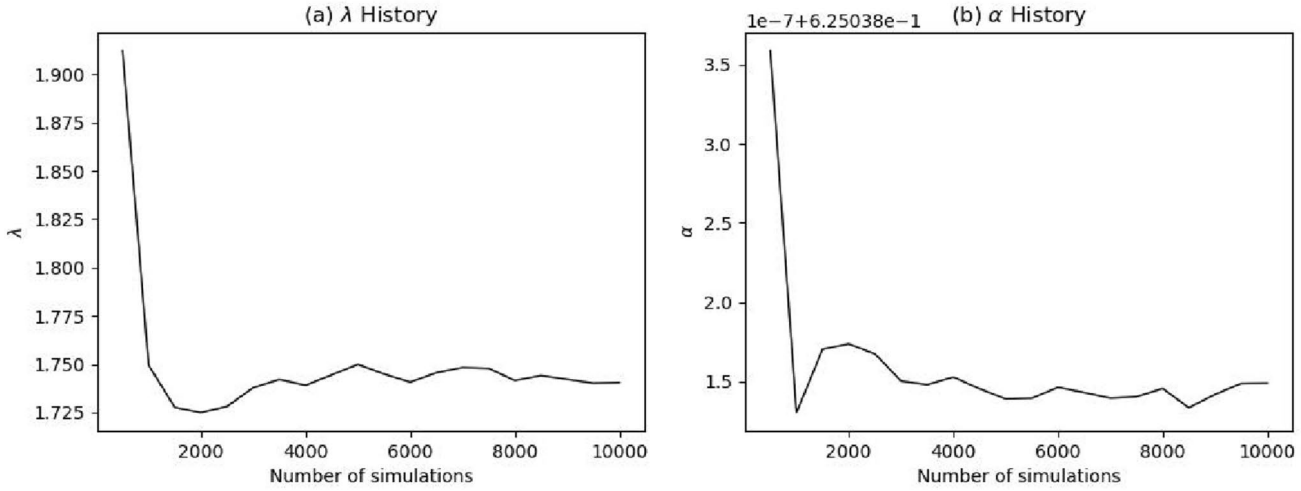

Fig. 10 Convergence history of the spatial regression parameters s

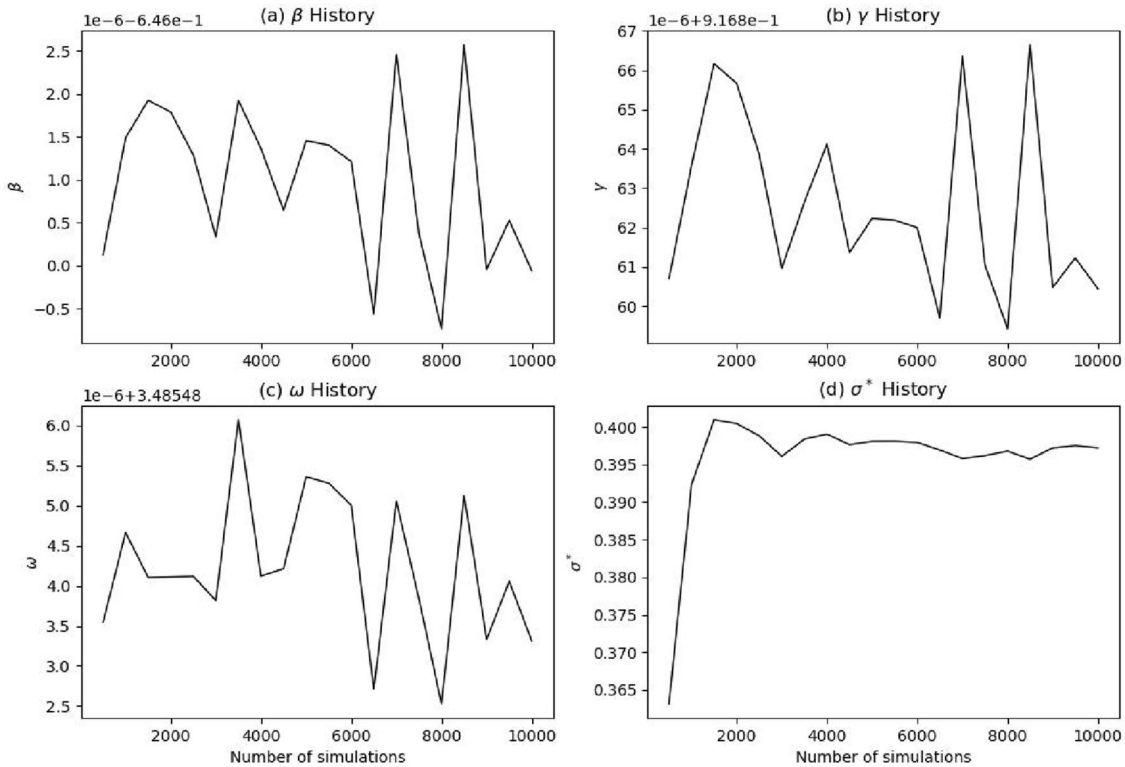

Fig. 11 Convergence history of the temporal regression parameters

Using the Galerkin method

$$\int R\eta \, \mathrm{d}y = 0, \quad \forall \eta \in V,$$

where V is the so-called finite-dimensional test space containing the interpolation functions; applying the boundary conditions and simplifying, one obtains the FEM formulation of the Euler–Bernoulli equation for a cantilever beam written in inner product notation as

$$\sum_{j}^{N} \langle \eta_i, \eta_j \rangle \ddot{w}_j + \sum_{j}^{N} \left\langle \eta_i'', \eta_j'' \right\rangle w_j = \langle \eta_i, q \rangle \quad i = 0, \ldots, N. \tag{35}$$

The normalised basis functions for a 1D beam elements are

$$\eta_1(y) = 1 - 3y^2 + 2y^3, \tag{36}$$

$$\eta_2(y) = y - 2y^2 + y^3, \tag{37}$$

$$\eta_3(y) = 3y^2 - 2y^3, \tag{38}$$

$$\eta_4(y) = y^3 - y^2. \tag{39}$$

For a one element FEM beam problem with two nodes, η_1 and η_2 correspond to the interpolation functions for the displacement and rotation, respectively at the first node, while η_3 and η_4 correspond to the interpolation functions for the displacement and rotation, respectively, at the second node. Equation (35) written in matrix notation is

$$\mathbf{A}\ddot{w} + \mathbf{B}w = \mathbf{F}, \tag{40}$$

where

$$A_{i,j} = \langle \eta_i, \eta_j \rangle$$
$$B_{i,j} = \left\langle \eta_i'', \eta_j'' \right\rangle$$
$$F_i = \langle \eta_i, q_i \rangle$$
$$w = \{w_i\} \quad i = 0, \ldots, N$$
$$\ddot{w} = \{\ddot{w}_i\} \quad i = 0, \ldots, N.$$

We solve for the term $\ddot{w}$ as

$$\ddot{w} = -\mathbf{A}^{-1}\mathbf{B}w + \mathbf{A}^{-1}\mathbf{F}. \tag{41}$$

From here, we can then apply a similar numerical scheme for the time integration as was done for the FD scheme by introducing the variable $v = \dot{w}$. Thus, (40) can be rewritten as a first-order ODE

$$\frac{\partial U}{\partial t} = \mathcal{M}U + \mathcal{F}, \tag{42}$$

where

$$U = \begin{pmatrix} w \\ v \end{pmatrix}, \qquad \mathcal{M} = \begin{pmatrix} 0 & 1 \\ -\mathbf{A}^{-1}\mathbf{B} & 0 \end{pmatrix}, \quad \mathcal{F} = \begin{pmatrix} 0 \\ \mathbf{A}^{-1}\mathbf{F} \end{pmatrix}. \tag{43}$$

Using the discretisations for the time and spatial variables equivalent to that applied to the FDM scheme, that is Eq. (23), we then conduct Monte Carlo simulations to obtain results for comparison with the FDM scheme. The result was filtered for the deflection as this research is not interested in the rotation at the nodes. To simplify the matter, we only compare the regression parameters in Eq. (32) as all other results can be derived from this.

Table 3 Comparison of the values of estimated parameters between FEM and FDM for the data at $t = T$

Parameters	FEM	FDM
$\tilde{\lambda}$	1.740502	1.740524
$\tilde{\alpha}$	0.625017	0.625038
$\tilde{\beta}$	−0.530752	−0.646000
$\tilde{\gamma}$	1.083184	0.916860
$\tilde{\Omega}$	3.277590	3.485483

Table 3 shows the comparison of the regression parameters. One can see the very close agreement between these results. It should be noted that while the results are comparable, the FEM scheme is much more computationally expensive than the FDM scheme. It is easy to see this by comparing the coupled PDE for the FDM scheme to that of FEM scheme, that is, Eqs. (20) and (42). One can see that the M matrix only requires assemblage once in the FDM scheme before the initiation of the MC simulations, while the FEM scheme requires an assemblage of matrices A and B once before MC simulation, the computation of the matrix multiplication of $A^{-1}B$ once before MC simulation and then the computation of $A^{-1}F$ for each MC simulation. These are the major differences in the implementation code for the MC simulations. For the same operating conditions, the run time of the FD scheme for ten thousand simulations is about 2 h 20 mins while that of the FE scheme is about 15 h which is much more than that of the FDM scheme.

6 Conclusion

The response of an Euler–Bernoulli beam subject to a stochastic disturbance in form of a white noise was investigated. The deflection was governed by the Stochastic Euler–Bernoulli Equation. A numerical approach based on a finite difference method was introduced and coupled with Monte Carlo method to solve an initial value problem of the stochastic partial differential equation. Ten thousand simulations were conducted to evaluate the statistics of the unknown beam deflection. The computational data were used for learning the solution behaviour by regression. There was a strong numerical evidence showing that the beam displacement follows a centred Gaussian process whose associated covariance function was computed from the samples and visualised in colour-map representations. Hence, it is concluded that a mild solution to the Stochastic Euler–Bernoulli Equation in the probability sense has been deduced by the designed approach that can be applied to other stochastic partial differential equations in the future. In practice, the

engineering safety assessment of a beam structure subject to a stochastic disturbance of white noise can be proceeded by considering the probability of the long-term deflection at the tip being no greater than 1% of the total beam length, that is

$$\mathbb{P}(w(y=1,t=T)<0.01) \tag{44}$$

which is computed by making use of (30). This value can be controlled to satisfy a confidence interval by restoring the standard deviation $\bar{\sigma}$ from (7) which in fact depends on the physical parameters from the original equation (1) in the non-dimensionalisation. Inversely, some intuitions regarding the requirements of the material properties are obtained.

The result was also compared to that obtained by the FEM scheme from which it was revealed that the FD scheme is much faster in terms of run time, easier to implement if one is coding from scratch and that results are comparable. Hence, it can be concluded that for such a simple structure, stochastic analysis using the FDM scheme is preferred.

As it relates to a BWT, the standard deviation $\hat{\sigma}$ can inform the design and layout of turbines in a wind farm, since it gives an indication of the deflection range. This is particularly important because the vortices formed around each BWT further affects the other BWTs around it which can be beneficial or detrimental to the energy conversion depending on layout design. Future studies can be conducted to examine the optimum power extraction by studying the allowable deflection range which then informs the arrangement of the BWTs in a wind farm.

Appendix

A modal composition

By the linear theory in which a separation of variables is conducted, the general solution to (4) can be written as

$$w(y,t)=\sum_{i=1}^{\infty} a_i(t)\phi_i(y), \tag{45}$$

where $a_i(t)$ are the unknowns and $\phi_i(y)$ are the eigenfunctions (also called normal modes) of Euler–Bernoulli equation for free vibration. These eigenfunctions take the form of

$$\phi_i(y)=b_i\cos\sqrt{\omega_i}y+c_i\sin\sqrt{\omega_i}y+d_i\cosh\sqrt{\omega_i}y+e_i\sinh\sqrt{\omega_i}y, \tag{46}$$

where the coefficients are determined by imposing the cantilever boundary conditions and ω_i are the natural frequencies. The first five natural modes are sketched in Fig. 12.

By making use of the orthogonality, the a_i must satisfy

$$\ddot{a}_i+\omega_i^2 a_i=\frac{\langle\phi_i,q\rangle}{\langle\phi_i,\phi_i\rangle}, \tag{47}$$

where $\langle\cdot,\cdot\rangle$ is an inner product defined by

$$\langle f_1,f_2\rangle=\int_0^1 f_1(\tilde{y})f_2(\tilde{y})d\tilde{y}. \tag{48}$$

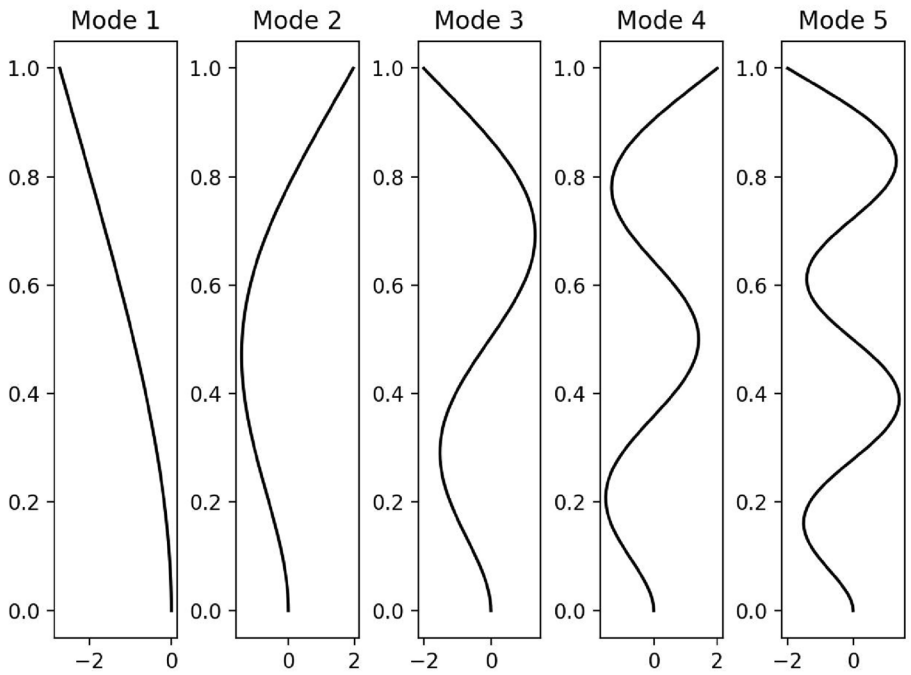

Fig. 12 The first five natural modes of the beam structure

If the load q is y-independent, the right-hand side of (47) can be further simplified. In the homogeneous case where $q = 0$, it can be easily found that $a_i = \sin \omega_i t$ by imposing the initial conditions. In practice, the series (45) is truncated after two terms for a good approximation.

It is noted that the Green's function for the second harmonic equation (47) is written as

$$G(t) = \frac{\sin(\omega_i t)}{\omega_i}\Theta(t), \tag{49}$$

with $\Theta(t)$ being the Heaviside step function, i.e., $\Theta(t) = 1$ if $t > 0$ and zero otherwise. Now, we consider the special case where $q = \xi(t)$ that is a Gaussian white noise only with respect to time. By making use of the Green's function (49), then the coefficient $a_i(t)$ takes the form of

$$a_i = \frac{\Gamma_i}{\omega_i}\int_0^t \sin\left(\omega_i\left(t - t'\right)\right)\xi(t')dt', \tag{50}$$

in which ξ is the generalised time derivative of a Wiener process, i.e., $\xi = \mathrm{d}W/\mathrm{d}t$, and

$$\Gamma_i = \frac{\langle \phi_i, \mathbb{1}\rangle}{\langle \phi_i, \phi_i\rangle}, \tag{51}$$

with $\mathbb{1}$ being the unity function. The solution (50) can be rewritten in Itô's sense as

$$da_i = -\frac{\Gamma_i}{\omega_i}\sin\left(\omega_i t\right)dW. \tag{52}$$

Substituting (52) back into the series solution (45) yields the solution of w

$$dw = A(y,t)dW, \tag{53}$$

$$A(y,t) = -\sum_{i=1}^{\infty}\frac{\Gamma_i}{\omega_i}\sin\left(\omega_i t\right)\phi_i(y). \tag{54}$$

It can be readily shown from (5354) that w follows a Gaussian process. The remaining task is to figure out its mean and autocovariance function. After some algebra, it is obtained that the a_i are all zero-mean and the covariance function of $C_{i,j}(t_1,t_2) = \mathbb{E}\left[a_i(t_1)a_j(t_2)\right]$ for $t_1 \le t_2$ is

$$C_{i,j}(t_1,t_2) = \frac{\Gamma_i\Gamma_j}{\omega_i\omega_j(\omega_i^2-\omega_j^2)}\Big[\omega_j\sin(\omega_i t_1)\cos(\omega_j t_2) - \omega_i\cos(\omega_i t_1)\sin(\omega_j t_2) + \sin(\omega_j(t_1-t_2))\Big]. \tag{55}$$

We follow to use (55) evaluate the following quantities:

– when $i = j$, it is obtained that

$$C_{i,i}(t_1,t_2) = \frac{\Gamma_i^2\left[\omega_i t_1\cos\left(\omega_i(t_1-t_2)\right) - \cos(\omega_i t_2)\sin(\omega_i t_1)\right]}{2\omega_i^3}; \tag{56}$$

– when $t_1 = t_2$, it is obtained that

$$C_{i,j}(t,t) = \frac{\Gamma_i\Gamma_j\left[\omega_j\sin\left(\omega_i t\right)\cos\left(\omega_j t\right) - \omega_i\cos\left(\omega_i t\right)\sin\left(\omega_j t\right)\right]}{\omega_i\omega_j(\omega_i^2-\omega_j^2)}. \tag{57}$$

– when $t_1 = t_2$ and $i = j$, the variance of $a(t)$ is found to be

$$\mathrm{Var}[a_i] = C_{i,i}(t,t) = \frac{\Gamma_i^2\left(\omega_i t - \cos\left(\omega_i t\right)\sin\left(\omega_i t\right)\right)}{2\omega_i^3}. \tag{58}$$

For computing the autocovariance of w, we approximate the solution by truncating the series after two terms, i.e., $w = a_1\phi_1 + a_2\phi_2$. Then, the autocovariance function is written as

$$\begin{aligned}&\mathbb{E}[w(y_1,t_1)w(y_2,t_2)]\\ &\quad= \phi_1(y_1)\phi_1(y_2)C_{1,1}(t_1,t_2) + \phi_2(y_1)\phi_2(y_2)C_{2,2}(t_1,t_2)\\ &\qquad+ \phi_1(y_1)\phi_2(y_2)C_{1,2}\left(t_1,t_2\right) + \phi_1(y_2)\phi_2(y_1)C_{1,2}\left(t_2,t_1\right).\end{aligned} \tag{59}$$

In particular, when $t_1 = t_2$ and $y_1 = y_2$, (59) is reduced to the variance of $w(y,t)$

$$\mathbb{E}[w(y,t)^2] = \phi_1(y)^2\mathrm{Var}[a_1] + \phi_2(y)^2\mathrm{Var}[a_2] + 2\phi_1(y)\phi_2(y)C_{1,2}(t,t). \tag{60}$$

Since $\mathbb{E}[a_i] = 0$, it can be easily deduced that the mean of the deflection over time t is zero, that is

$$\mathbb{E}[w(y,t)] = 0. \tag{61}$$

We have developed a simple valid theory for predicting the mean and the covariance of the unknown w, that has been shown to follow a Gaussian process, in the special case where the random external force has no spatial variation. For the general case where ξ depends on both y and t, the calculation turns out to be tedious, and the solution becomes much more complex which makes it impractical for theoretical estimations. Instead, the regression model, i.e., Eq. (31), presented in Sect. () derived from the numerical method presented is a preferred alternative.

Declarations

Conflict of interest The authors have no relevant financial or non-financial interests to disclose.

References

1. Bahadur I (2022) Dynamic modeling and investigation of a tunable vortex bladeless wind turbine. Energies 15(18):6773
2. Bertini L, Cancrini N (1995) The stochastic heat equation: Feynman-Kac formula and intermittence. J Stat Phys 78(5–6):1377–1401
3. Bertini L, Cancrini N, Jona-Lasinio G (1994) The stochastic Burgers equation. Commun Math Phys 165(2):211–232
4. Cajas JC, Shah S, Houzeauxa G, Yáñez DJ, Mier-Torrecilla M (2016) SHAPE project vortex bladeless: parallel multi-code coupling for fluid-structure interaction in wind energy generation, EU's Horizon 2020 research and innovation programme. Available online at www.prace-ri.eu
5. Chizfahm A, Yazdi EA, Eghtesad M (2018) Dynamic modeling of vortex induced vibration wind turbines. Renew Energy 121:632–643
6. Da Prato G, Debussche A, Temam R (1994) Stochastic Burgers' equation. Nonlinear Differ Equ Appl 1(4):389–402
7. Davari SM, Malekinejad M, Rahgozar R (2019) Static analysis of tall buildings based on Timoshenko beam theory. Int J Adv Struct Eng 11(4):455–461
8. Davari SM, Rahgozar R, Maleknejad M (2019) A simple method for static analysis of tubular high-rise buildings using Timoshenko beam theory. Int J Eng Technol 11(3):563–575
9. Foda MA, Abduljabbar Z (1998) A dynamic green function formulation for the response of a beam structure to a moving mass. J Sound Vib 210(3):295–306
10. Gikhman II, Skorohod AV (1972) Stochastic differential equations. Springer
11. Giosan I, Eng P (2013) Vortex shedding induced loads on free standing structures. Structural Vortex Shedding Response Estimation Methodology and Finite Element Simulation, 42
12. Higham DJ (2001) An algorithmic introduction to numerical simulation of stochastic differential equations. SIAM Rev 43(3):525–546
13. Ortner N, Wagner P (1990) The Green's functions of clamped semi-infinite vibrating beams and plates. Int J Solids Struct 26(2):237–249
14. Rajmani A, Guha PP (2015) Analysis of wind & earthquake load for different shapes of high rise building. Int J Civ Eng Technol 6(2):38–45
15. Stafford Smith B, Coull A (1991) Tall building structures: analysis and design
16. Takabatake H, Kitada Y, Takewaki I, Kishida A (2019) Simplified dynamic analysis of high-rise buildings: applications to simplified seismic diagnosis and retrofit using the extended rod theory. Springer
17. Tandel R, Shah S, Tripathi S (2021) A state-of-art review on Bladeless Wind Turbine. J Phys Conf Ser 1950:012058
18. Watanabe K (2015) Green's functions for beam and plate. Integral transform techniques for green's function. Springer, Cham, pp 139–152
19. Williamson CHK, Govardhan R (2004) Vortex-induced vibrations. Annu Rev Fluid Mech 36:413–455
20. www.bsc.es